Gold Bulletin (2019) 52:105–114
https://doi.org/10.1007/s13404-019-00259-9

ORIGINAL PAPER

Thermal stability of oxide-supported gold nanoparticles

Nazila Masoud[1] · Tomas Partsch[1] · Krijn P. de Jong[1] · Petra E. de Jongh[1]

Received: 28 August 2018 / Accepted: 23 April 2019 / Published online: 16 May 2019

Abstract

In this study, we report on the influence of support and gas atmosphere on the thermal stability of Au nanoparticles on oxidic supports. All samples were prepared with a modified impregnation method and have initial Au particle sizes in the range of 3–4 nm. We observed that in air, Au nanoparticles on SiO_2 and Al_2O_3 are thermally much more stable than Au nanoparticles on TiO_2. For instance, upon treatment up to 700 °C, on SiO_2, Au particles grew from 4 to 6 nm while on TiO_2 from 3 to 13 nm. For Au nanoparticles on TiO_2, growth is accelerated by oxidizing atmospheres and the presence of water and/or chloride. On non-reducible supports and in non-oxidizing atmosphere, the supported Au nanoparticles were remarkably stable. The insight into the growth of oxide-supported Au nanoparticles in reactive atmosphere offers an additional tool for a rational choice of a support for high-temperature gas-phase reactions involving gold nanocatalysts.

Keywords Au · Sintering · Support effect · Atmosphere effect

Introduction

By development of environmental protection regulations, less CO emission is demanded. Most of the CO emission occurs when the engine is still cold [1]. Gold is the most active catalyst for CO oxidation at room temperature which makes Au catalysts very interesting for this application [2–6]. However, when the engine becomes hot, it reaches the temperatures as high as 700 °C, and high-temperature treatment often causes growth of Au nanoparticles [7–14]. For bulk Au, the melting point is 1064 °C, and the Hüttig temperature at which surface atoms become mobile is 319 °C. For Au nanoparticles, the melting point is even lower [15]. Hence, one can expect the growth of Au nanoparticles at elevated temperatures. Deactivation due to particle growth is irreversible and detrimental to the long-term activity of the catalyst. Different state-of-the-art strategies [16–19] have been employed to combat the particle growth. For instance, a high thermal stability of Au nanoparticles on combinatory TiO_2/SiO_2 support [20], hydroxyapatite/TiO_2 support [21], nanorods of TiO_2 [22], and perovskite support [23] has been reported.

Supports stabilize Au nanoparticles by enhancing inter-particle spacing and sometimes by metal support interaction [24, 25]. For instance, Au nanoparticles on Al_2O_3 have shown excellent stability upon treatment at 650 °C under oxidizing conditions [2, 26, 27]. However, Au/TiO_2 catalyst, which is the most studied type of Au catalyst, is known to grow during CO oxidation [28–30] as well as during high-temperature treatment under oxidizing atmosphere [7], though the exact conditions that cause the growth are under discussion [29, 30]. Au/TiO_2 catalysts are known to deteriorate during storage, as they are light and moisture sensitive [31, 32]. The stability of Au/SiO_2 is under debate [33–40]. Though there are some examples of stability and/or instability of supported Au nanoparticles, the influence of the nature of the support and reaction conditions on the stability is not well understood.

More importantly, the mechanisms that are involved in Au particle growth under different conditions are unclear. Particle growth can take place via two major mechanisms [41]. The first one involves nanoparticle diffusion over the support surface and coalescence to form larger particles (particle diffusion and coalescence). The diffusion is more likely for smaller particles, and it is accelerated when the temperature increases, roughly following Arrhenius behavior [42]. Near the Tamman temperature, at which the metal atoms acquire sufficient energy for their bulk mobility, particle diffusion becomes more dominant.

Electronic supplementary material The online version of this article (https://doi.org/10.1007/s13404-019-00259-9) contains supplementary material, which is available to authorized users.

✉ Petra E. de Jongh
p.e.dejongh@uu.nl

[1] Inorganic Chemistry and Catalysis, Debye Institute for Nanomaterials Science, Utrecht University, 3584 CG Utrecht, the Netherlands

Secondly, larger particles grow at the expense of smaller particles (Ostwald ripening) [11, 41]. The driving force is that the higher surface energy of low coordinated metal atoms at the surface of small particles destabilizes the small particles and makes the larger particles, compared with smaller particles, energetically more favorable. Hence, metal species detach from small particles, diffuse over the support or through the vapor phase, and can attach to larger particles with a lower chemical potential. This leads to the growth of larger particles at the expense of smaller particles.

According to fundamental studies by Wynblatt and Gjostein [42], Ostwald ripening can have two possible rate-limiting steps: detachment of metal atom from small particles in form of mobile species, the so-called interface-controlled regime, and diffusion of mobile species from smaller particles to the larger one, the so-called diffusion-controlled regime. Mobile species can be metal atoms or metal ions of metal-containing molecules. In the latter, the metal or metal ions are complexed and stabilized by surface groups and/or species from the gas phase that act as ligands. Ligands decrease the activation energy for the detachment of a metal (ion) from a nanoparticle. Hence, the formation of mobile species depends on the presence of reactive gases, certain surface groups, and/or oxidizing or reducing conditions [25]. For example, fast growth of Pt/Al_2O_3 under O_2 atmosphere was attributed to the formation of volatile PtO_2 species under oxidizing atmosphere as well as a high diffusivity of PtO_2 over the support surface [43]. The growth of Ni nanoparticles during the methanation reaction was ascribed to the formation of gas-phase $Ni(CO)_5$ as mobile species [44]. The most likely mobile species in different reactive conditions can be predicted by calculating thermodynamics and energy barriers for the diffusion of the different possible complexes. For instance, based on DFT calculations, CuCO species were assumed to be the mobile species in Cu/ZnO catalysts under methanol synthesis conditions and during water gas shift reaction [45].

To the best of our knowledge, there is no systematic study on the growth of Au nanoparticles on different supports that are prepared with the same method and have similar composition, support porosity, and initial Au particle size. Catalyst preparation method affects the stability of supported nanoparticles by influencing catalyst properties such as distribution of Au particles over the support and the concentration of contaminants like Cl that can promote particle growth [46]. A uniform spatial distribution of particles, with maximum inter-particle distances of supported nanoparticles, and a very narrow particle size distribution play an important role in minimizing particle growth [44, 47].

In this study, we report on the growth of Au nanoparticles on supports with different properties using non-reducible ones (SiO_2 and γ-alumina) and a reducible one (TiO_2). We employed a modified incipient wetness impregnation method to prepare 3 to 4 nm Au nanoparticles on TiO_2, Al_2O_3, and SiO_2 supports [48]. The effect of different reactive gases on the particle growth was investigated. The activation energies of particle growth for Au on different supports and in different reactive gases were experimentally obtained as well.

Experimental

Sample preparation

Commercially available supports, TiO_2 (rutile, BET surface area of 30 $m^2\ g^{-1}$, pore volume of 0.12 mL g^{-1}, Sigma-Aldrich), SiO_2 (Aerosil, BET surface area of 50 $m^2\ g^{-1}$, pore volume of 0.12 mL g^{-1}, Evonik), and Al_2O_3 (gamma phase, BET surface area of 120 $m^2\ g^{-1}$, pore volume of 0.46 mL g^{-1}, Alfa-Aesar) were used. Not the most commonly used P25, TiO_2 with mixed phases of anatase and rutile, but instead pure rutile was used because at 500 °C and above, anatase phase transforms to rutile phase [49], and this change in support phase could contribute to particle growth.

Gold was deposited on the supports by a modified incipient wetness impregnation method developed by Delannoy et al. [48]. In a typical preparation, the support (1 g) was dried under vacuum at 200 °C and was impregnated with an aqueous Au solution (appropriate concentration of $HAuCl_4{\cdot}3H_2O$, Sigma-Aldrich) to prepare 1 wt% Au on TiO_2 and SiO_2 and 4 wt% Au on Al_2O_3. The sample was aged at room temperature under vacuum for 1 h and then washed twice with ammonia solution (30 mL each time, 1 M) to remove Cl and twice with water (30 mL each time) at RT. Each time, the solid was recovered by centrifugation. The Au/SiO_2 sample was washed with diluted ammonia solution at lower pH (pH = 8) to remove Cl and to avoid dissolution of SiO_2 as well. The sample was then dried under vacuum at room temperature for 48 h or was dried in a freeze drier at − 20 °C under 0.1 mbar vacuum for 17 h. The dried samples were further treated in air (100 mL min^{-1}) from RT to 300 °C (ramp 2 °C min^{-1}) and kept at 300 °C for 4 h before cooling down and stored in a desiccator in the dark.

Another sample of Au/TiO_2 was prepared with the method of deposition-precipitation with urea [46] to promote preparation of a Cl-free sample. In a typical preparation, the support (1 g, rutile, Sigma-Aldrich) was dispersed in water (100 mL) in a 500-mL polyethylene bottle, and the reaction mixture was stabilized in an oil bath at 80 °C. An aqueous Au solution (2 mL, 0.027 M, $HAuCl_4{\cdot}3H_2O$ precursor, Sigma-Aldrich) and urea (300 mg) were added. The reaction mixture was stirred for 16 h in a closed container at 80 °C in the dark. Then, the solid was recovered by centrifugation and was washed eight times with water (40 mL each time) at RT. The sample was then dried in a freeze drier at − 20 °C under 0.1 mbar vacuum for 17 h. The dried samples were further reduced in H_2 (100 mL min^{-1}) from RT to 300 °C (ramp

2 °C min^{-1}) and kept at 300 °C for 2 h before cooling down and stored in a desiccator in the dark.

Characterization

Elemental analysis was performed on an inductively coupled plasma-mass spectrometer (Mikroanalytisches Laboratorium Kolbe, Germany) after destruction of the samples at high temperature and pressure. Chloride content of the samples was determined by ion chromatography (Mikroanalytisches Laboratorium Kolbe). Transmission electron microscopy (TEM) imaging was performed on a Tecnai 12 (FEI) microscope operated at 120 kV. Particle sizes were determined from the micrographs as $\sum n_i d_i / \sum n_i$, where d_i is the diameter of typically 200–300 individual particles on different areas of the sample. High-angle annular dark-field scanning transmission electron microscopy (HAADF-STEM) was performed on a Talos F200X microscope operated at 200 kV. STEM image processing was carried out using Tecnai Imaging Analysis (TIA).

Thermal treatment

The thermal treatment of the samples was performed either under static condition or in a gas flow. The experiments under static condition were performed in a temperature-calibrated muffle furnace. Typically, 40 mg of the sample was heated in air from RT to 500, 600, or 700 °C (ramp 5 °C min^{-1}) and kept at the specified temperature for 4 h. The experiments in flows of different gases, compressed air (wet air), synthetic air (dry air), H_2, N_2, or N_2 that was bubbled through water at RT (100 mL min^{-1}), were performed on 200 mg of the sample in a plug flow reactor with diameter of 2 cm at 500 °C with the same heating program. The experiments in flow of H_2 at 600 and 700 °C were done in a crucible with a horizontal tubular furnace under the flow of 25 mL min^{-1} to imitate the static condition in air. The experiments and analytical measurements were performed at least twice to ensure reproducibility of the results.

Activation energy of particle growth was calculated from the Arrhenius plots (ln (*particle growth rate*) versus 1/*T*), where *particle growth rate* is estimated from the changes in particle sizes upon 4 h of thermal treatment at different temperatures (*T*).

Results

Sample characteristics

Figure 1 shows transmission electron micrographs of Au nanoparticles supported on three different supports. Particle sizes for these prepared samples were between 2.5 and 4.0 nm (Table 1). Determination of particle sizes relied on TEM micrographs, as crystallite sizes could not be derived from X-ray diffraction patterns owing to low Au loading and overlap of diffraction patterns. With bright-field TEM, particle sizes were difficult to determine for the Au/TiO_2 sample due to a low contrast. Therefore, in this case, additional high-angle annular dark-field scanning transmission electron microscopy (HAADF-STEM) was employed. HAADF-STEM micrographs (Figure S.1) showed particle size of 2.6 ± 0.6 nm for the Au/TiO_2 which confirms the accuracy of the particle size obtained by bright-field TEM.

Table 1 presents the structural properties of the samples. The Au loading for each sample was chosen based on the BET surface areas of the corresponding supports aiming for similar inter-particle distances for all samples. For instance, the surface area of the commercially available γ-Al_2O_3 is four times higher than that of TiO_2; hence, a four times higher Au loading for the Au/Al_2O_3 was targeted. The average inter-particle distances were between 30 and 50 nm for all the supported Au nanoparticles. Elemental analysis showed that targeted Au loadings were achieved and the Cl content of all samples is between 0.3 and 0.4 wt%. For comparison, an Au/TiO_2 sample with negligible Cl content was prepared by the method of deposition-precipitation with urea. Hence, all the supported Au samples had similar properties, though the as-prepared Au nanoparticles on TiO_2 had slightly smaller sizes than the two other samples.

Impact of the support on the thermal stability

Figure 2 shows TEM micrographs of the Au/TiO_2 sample upon treatment to temperatures up 700 °C in air. Additionally, Figure S.2 shows the ones for Au/SiO_2 and Au/Al_2O_3. These figures demonstrated that all supported Au nanoparticles have grown upon thermal treatment. However, growth for Au nanoparticles on TiO_2 was more pronounced (Fig. 2).

Figure 3 shows, in summary, the evolution of particle size distributions and shows that the particles grew with increasing temperature. The particles for the Au/TiO_2 sample were initially smaller than those for the Au/SiO_2 and Au/Al_2O_3 samples, but they grew more upon thermal treatments: 2.1-fold increase in diameter at 500 °C, 2.4-fold at 600 °C, and 5.0-fold at 700 °C. Furthermore, the particle size distribution was broadening. The Au nanoparticles on SiO_2 and Al_2O_3 grew too, but to a limited extent: for the Au/SiO_2: no significant growth at 500 °C, 1.1-fold at 600 °C, and 1.8-fold at 700 °C. The particle size for the Au/TiO_2-DPU that contained no Cl increased too: 1.7-fold at 500 °C, 2.4-fold at 600 °C, and 4.3-fold at 700 °C. This particle growth was less than for the Au/TiO_2 with some Cl, in agreement with the literature that suggests Cl residue enhances growth of Au nanoparticles on TiO_2 [50]. Nevertheless, Au nanoparticles on TiO_2, even with

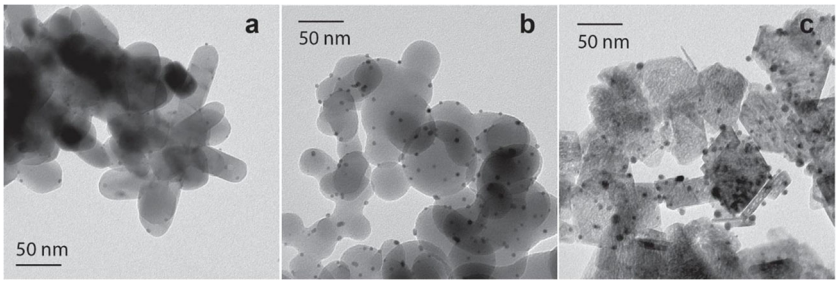

Fig. 1 Transmission electron micrographs for the 0.9 wt% Au/TiO_2 (**a**), 1.0 wt% Au/SiO_2 (**b**), and 4.0 wt% Au/Al_2O_3 (**c**)

negligible Cl content, were thermally less stable than the ones on SiO_2 and Al_2O_3 in air.

Effect of atmosphere

Figure 4 compares the thermal stability of Au nanoparticles on TiO_2 and SiO_2 under different atmospheres, varying from reducing (a flow of H_2) via inert (a flow of N_2) towards oxidizing (a flow of wet air). First, for the Au/TiO_2, the particle growth was negligible in either H_2 or N_2, but it became more pronounced in the presence of water vapor (~ 2 mol% water in N_2, 1.6-fold increase) and in the presence of dry air (3.1-fold increase). It means that presence of O_2 and/or water accelerated the thermal growth of Au nanoparticles on TiO_2 supports. In contrast, no significant difference in particle growth, and in both cases a high thermal stability, was observed either in inert atmosphere or in the presence of H_2. This observation excluded strong metal support interaction between Au and the reducible TiO_2 support, which typically occurs under reducing conditions, as a reason for the high stability of Au nanoparticles on TiO_2 in the flow of H_2. Hence, the particle growth occurred for the Au/TiO_2 only in the presence of O_2 and/or water.

In contrast, Fig. 4 shows that for the Au/SiO_2, the particle growth was negligible under all atmospheres tested. In summary, the growth of Au nanoparticles was influenced by the atmosphere only when they were supported on the TiO_2, but not when they were supported on SiO_2, and particle growth was more pronounced in an oxidizing atmosphere.

Figure 5 shows the Arrhenius plots for rates of Au nanoparticles growth (dR/dt, where R is the particle diameter and t is time) on the TiO_2 and SiO_2 under different atmospheres. The dR/dt was extracted from plots in Figure S.3. The activation energies of particle growth (E_a) estimated from the plots are given in Fig. 5 as well. In air, E_a for Au/TiO_2 (36 ± 10 kJ mol^{-1}) was lower than the one for Au/SiO_2 (86 ± 14 kJ mol^{-1}). However, in H_2, the E_a was similar for Au nanoparticles on both TiO_2 and SiO_2 (80 ± 6 vs 81 ± 13 kJ mol^{-1}). Notably, E_a for the Au/SiO_2 under different atmospheres was also similar. This suggests that the rate-limiting step in particle growth for the Au/TiO_2 and Au/SiO_2 in H_2 and for the Au/SiO_2 in air might be similar whereas rate of Au nanoparticle growth on TiO_2 is apparently not or much less limited by this step in air. This will be discussed in more detail in the "Discussion" section.

Discussion

There are a few reports on the growth of Au nanoparticles supported on TiO_2 upon high-temperature treatment and under oxidizing atmosphere [7]. Akita et al. reported that Au nanoparticles of 2.1 nm on TiO_2 grew to 9.7-nm particles upon calcination in air at 600 °C for 4 h [32]. A high thermal stability of Au nanoparticles on Al_2O_3 upon treatment at 650 °C in three-way catalysis conditions [2, 27] and in a flow of O_2 [26] was previously reported. There is no consensus on the thermal stability of Au nanoparticles on SiO_2. Some reports suggested that they grow [33–38]. For instance, Bore et al. [37] showed that Au nanoparticles of around 1 nm on mesoporous SiO_2 grew to in average 6 nm upon H_2 exposure

Table 1 Structural properties of the samples

	BET surface area (m^2 g^{-1})	Au loading (wt%)	Cl content (wt%)	Particle size (nm)
Au/TiO_2	30	0.9	0.4	2.7 ± 1.2
Au/TiO_2-DPU[a]	30	1.0	< 100 ppb[b]	2.3 ± 0.6
Au/SiO_2	50	1.0	0.4	3.6 ± 0.9
Au/Al_2O_3	120	4.0	0.3	3.8 ± 1.3

[a] Sample was prepared by deposition-precipitation with urea. All other samples were prepared by modified incipient wetness impregnation

[b] Below the detection limit

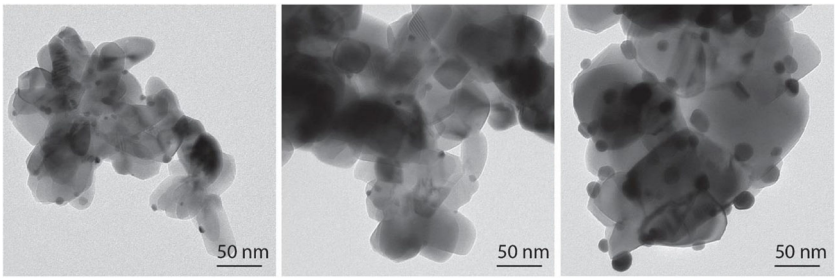

Fig. 2 Transmission electron micrographs of 0.9 wt% Au/TiO_2 that has been treated, from left to right, upon treatment at 500, 600, and 700 °C in static air for 4 h

at 200 °C. In contrast, some other reports claimed that if the Au/SiO_2 contains little or no Cl, the Au nanoparticles are actually stable upon O_2 exposure at 500 °C [39, 40]. In the latter case, the high stability of Au nanoparticles on SiO_2 was attributed to a strong bond between Au and defects on the surface of SiO_2. It was proposed that the defects on the surface were made during deposition of Au on the SiO_2 by magnetron sputtering [40]. Barret et al. showed as well that enhanced defect sites on the TiO_2 surface make the supported Au nanoparticles thermally stable [22]. All mentioned reports are examples obtained under catalysis conditions on powder catalysts. On 2D model systems in vacuum, the interaction of Au with reducible supports like TiO_2 is suggested to provide stable Au nanoparticles [28, 51]. Accordingly, Au on non-reducible Al_2O_3 and SiO_2 supports is suggested to be less stable [16]. Our study clearly proves a higher thermal stability of Au nanoparticles on the non-reducible supports SiO_2 and Al_2O_3 than on TiO_2.

It is known that gas atmosphere can affect the growth of metal nanoparticles. Oxidizing atmospheres typically induce faster rates of particle growth than reducing atmospheres [43, 52]. Particularly for Au/TiO_2, it was reported that Au particle sizes are smaller if the sample is prepared in H_2 or Ar than when it is prepared in O_2 [31]. However, to the best of our knowledge, this is the first report that shows that the situation is different for different supports and that the Au, regardless of the atmosphere, is thermally stable on the SiO_2 support.

This is also the first time that the activation energies of particle growth under conditions closer to catalytic reaction conditions for Au on different supports and in different reactive gases are obtained. For comparison, the activation energy of particle growth for Ni nanoparticle catalysts under steam reforming condition was estimated to be 46 ± 8 kJ mol^{-1} [53]. The activation energy of particle growth for Au particles supported on single-crystal TiO_2 (110) under ultra-high vacuum was estimated as high as 280 kJ mol^{-1} [54, 55]. Notably, this higher value was obtained under UHV conditions rather than relevant catalytic conditions and on atomically flat clean surfaces rather than powder supports with surface groups and adsorbed molecules [54]. Hence, one can conclude that under conditions closer to the catalytic reaction conditions, the activation energy of particle growth is much lower and often particle growth is much faster than for 2D model systems in vacuum.

As mentioned in the "Introduction" section, particle growth can take place via two mechanisms: particle diffusion and coalescence or Ostwald ripening. Our results suggest three main conclusions on involved particle growth mechanisms: First, particle diffusion and coalescence as a major particle growth mechanism is unlikely. The distance between the particles is estimated to be around 50 nm for all the samples. Our previous reports on the growth of Cu nanoparticles during methanol synthesis showed a very strong dependence of particle diffusion and coalescence on inter-particle size with diffusion dominating at such large distances unlikely [47, 56]. Furthermore, DFT calculations showed that Au nanoparticles interact much stronger with TiO_2 surfaces than with SiO_2 surfaces [40]. If high-temperature treatments do not induce particle diffusion and coalescence for the Au nanoparticles on SiO_2, it is unlikely that particle diffusion and coalescence take place for the TiO_2 surfaces under similar conditions. Therefore, particle growth by Ostwald ripening most likely is the main particle growth mechanism at least under oxidizing atmospheres. It has been suggested that particle growth by Ostwald ripening is also the main growth mechanism for the Au on single-crystal TiO_2 (110) under ultra-high vacuum upon a high-temperature treatment [28].

Identifying the mobile species is not trivial [57]. Because of the large influence of the chemical nature of the support on particle growth observed in this study, a second conclusion would be that the mobile species are at the support surface rather than in gas phase. At temperatures of 177 °C and above, Au does not form any stable oxides [58] or volatile compounds like Pt does in the form of PtO_2. The energy required to remove a metal atom from a metal particle is high, close to the heat of sublimation of metals [53], which is 368 kJ mol^{-1} for Au [54, 55]. The fact that the experimentally observed E_a for growth of Au nanoparticles are an order of magnitude lower leads to a third conclusion that Au is unlikely to detach from a nanoparticle in metallic form. Furthermore, using the Kelvin equation, saturation pressures for Au nanoparticles with different sizes at different temperatures were calculated (supporting information, estimation of the diffusion of atomic Au in the gas phase at different temperatures). From the

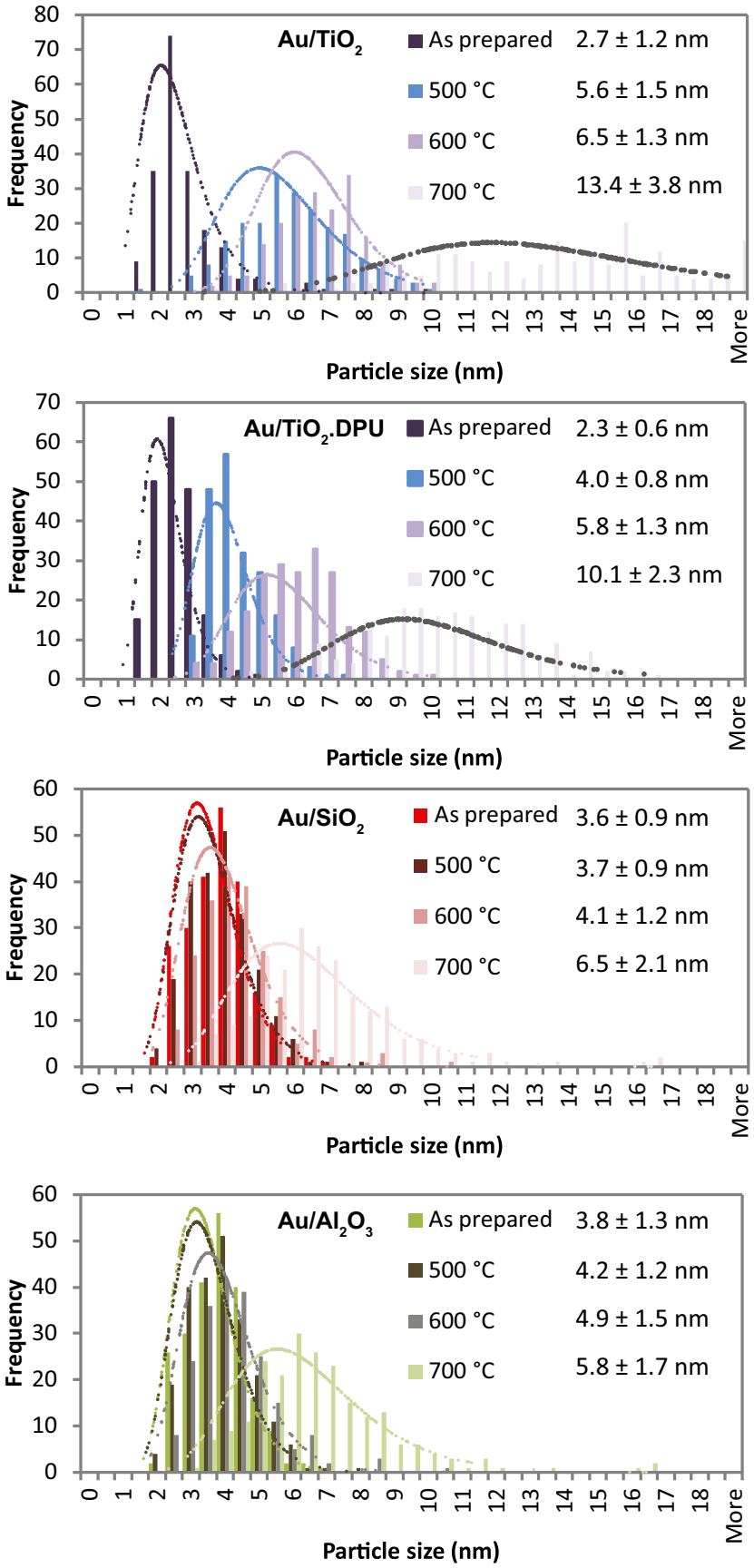

Fig. 3 Evolution of particle size distributions and log normal fits for the as-prepared Au on TiO_2, SiO_2, and Al_2O_3 as well as for the samples that have been treated at 500, 600, and 700 °C in static air for 4 h

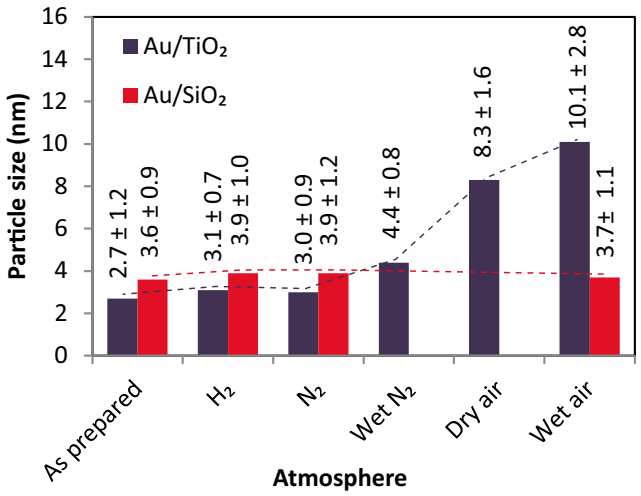

Fig. 4 Effect of gas composition on the size of Au nanoparticles on TiO_2 or SiO_2 that have been treated at 500 °C in different flows of gases (100 mL min^{-1}) for 4 h

difference in the saturation pressures of the Au vapor around the small and large Au nanoparticles, the diffusion rate for atomic Au in the gas phase was estimated. The calculation showed that Ostwald ripening via the atomic Au in the gas phase is not a main factor in explaining the observed particle growth. The observation that the formation and/or diffusivity of mobile species is accelerated on TiO_2 and under oxidizing atmosphere as well as in the presence of Cl^- ions strongly suggests adsorbed complexed and oxidized Au species being the mobile species.

It is remarkable that the E_a for particle growth in air on Au/TiO_2 is smaller than that on Au/SiO_2. This means that the formation and/or the diffusivity of the Au-complex mobile species is less favorable on SiO_2. It is known, for instance, from CO oxidation studies [59–69], that Au and TiO_2 have a very specific interaction, which leads to very active and possibly cationic gold species at the interface between the two, which might also play a role in diminishing the thermal stability of the TiO_2-supported particles. It is remarkable that the E_a under other conditions, whether on SiO_2 in either reducing or oxidizing conditions, or on TiO_2 under reducing conditions, are all similar and in the range of 80–86 kJ/mol. This suggests that in the absence of this specific Au-TiO_2 interaction in oxidizing atmosphere, particle growth follows a similar mechanism. Tentatively, we propose that under oxidizing conditions cationic Au species are mobile species that are stabilized on TiO_2 to a larger extent that on SiO_2 in line with the lower activation energy for growth on the former (Fig. 5). In any case, the fact that Au catalysts on non-reducible supports show such high thermal stability, even though they often show lower activities than on reducible supports like TiO_2 [70], is a very relevant consideration for the potential application of Au nanoparticles in gas-phase catalysis.

Conclusion

For the first time, the thermal growth of Au nanoparticles on different oxidic supports and under different reactive atmospheres was studied. Similar initial particle sizes, in the 2.5–4-nm range, allowed direct comparison for the different supports. All supported Au nanoparticles grew upon thermal treatment. Particle growth on TiO_2 was much more pronounced than that on either SiO_2 or Al_2O_3. Particle growth on TiO_2 was particularly enhanced by an oxidizing atmosphere, the presence of water, and/or the presence of Cl^-. Particle growth by Ostwald ripening involving cationic gold species complexed by ligands was the most likely dominating growth mechanism. On non-reducible supports and in non-oxidizing atmosphere, the supported Au nanoparticles were remarkably stable. These results provide a better understanding of the growth of supported Au nanoparticles, and tools for a rational choice of a support for high-temperature gas-phase reactions involving gold catalysts.

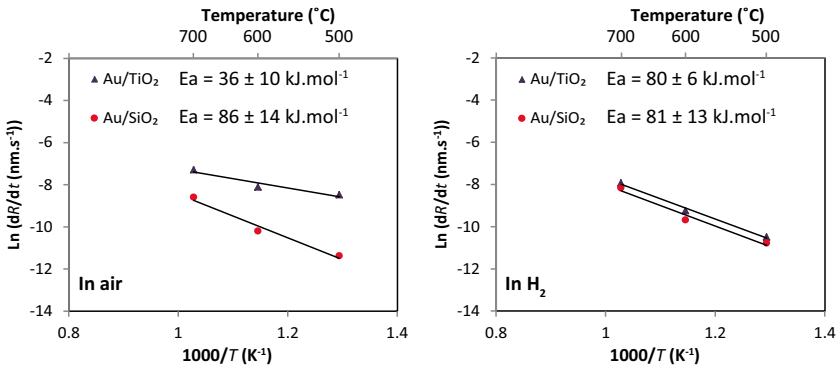

Fig. 5 The Arrhenius plots of the rates of Au nanoparticles growth on TiO_2 and SiO_2 in static air and in a flow of H_2 (25 mL min^{-1}, in a tube furnace) after 4 h. *R* is particle size and *t* is time

Acknowledgments We gratefully acknowledge Jessi van der Hoeven for the HAADF-STEM imaging and Neda Kordalivand from the Department of Pharmaceutical Sciences for operating the freeze drier.

Funding information This study received overall funding of the project from NWO-Vici (16.130.344). Krijn P. de Jong received support from the European Research Council, EU FP7 ERC Advanced Grant No. 338846.

Compliance with ethical standards

Conflict of interest The authors declare that there are no conflicts of interest.

References

1. Methods for monitoring and diagnosis the efficiency of catalytic converters: a patent-oriented survey (1998), vol 115. studies in surface science and catalysis. Elsevier. https://doi.org/10.1016/s0167-2991(98)80929-4
2. Ulrich V, Moroz B, Sinev I, Pyriaev P, Bukhtiyarov V, Grunert W (2017) Studies on three-way catalysis with supported gold catalysts. Influence of support and water content in feed. Appl Catal, B 203:572–581. https://doi.org/10.1016/j.apcatb.2016.10.017
3. Bauer JC, Toops TJ, Oyola Y, Parks Ii JE, Dai S, Overbury SH (2014) Catalytic activity and thermal stability of Au–CuO/SiO_2 catalysts for the low temperature oxidation of CO in the presence of propylene and NO. Catal Today 231:15–21. https://doi.org/10.1016/j.cattod.2014.01.040
4. Haruta M (2014) Chance and necessity: my encounter with gold catalysts. Angew Chem Int Ed Engl 53(1):52–56. https://doi.org/10.1002/anie.201305987
5. Min BK, Friend CM (2007) Heterogeneous gold-based catalysis for green chemistry: low-temperature CO oxidation and propene oxidation. Chem Rev 107(6):2709–2724. https://doi.org/10.1021/cr050954d
6. Scurrell MS (2017) Thoughts on the use of gold-based catalysts in environmental protection catalysis. Gold Bull 50(1):77–84. https://doi.org/10.1007/s13404-017-0194-z
7. Ma Z, Dai S (2014) Stabilizing gold nanoparticles by solid supports. In: Ma Z, Dai S (eds) Heterogeneous gold catalysts and catalysis. RSC, Stratford-upon-Avon, pp 1–26. https://doi.org/10.1039/9781782621645-00001
8. Chen C, Nan C, Wang D, Su Q, Duan H, Liu X, Zhang L, Chu D, Song W, Peng Q, Li Y (2011) Mesoporous multicomponent nanocomposite colloidal spheres: ideal high-temperature stable model catalysts. Angew Chem Int Ed Engl 50(16):3725–3729. https://doi.org/10.1002/anie.201007229
9. Wei Y, Zhao Z, Jin B, Yu X, Jiao J, Li K, Liu J (2015) Synthesis of AuPt alloy nanoparticles supported on 3D ordered macroporous oxide with enhanced catalytic performance for soot combustion. Catal Today 251:103–113. https://doi.org/10.1016/j.cattod.2014.08.034
10. Laveille P, Guillois K, Tuel A, Petit C, Basset JM, Caps V (2016) Durable PROX catalyst based on gold nanoparticles and hydrophobic silica. Chem Commun (Camb) 52(15):3179–3182. https://doi.org/10.1039/c5cc09561a
11. Simonsen SB, Chorkendorff I, Dahl S, Skoglundh M, Sehested J, Helveg S (2011) Ostwald ripening in a Pt/SiO_2 model catalyst studied by in situ TEM. J Catal 281(1):147–155. https://doi.org/10.1016/j.jcat.2011.04.011
12. Zhao K, Qiao B, Wang J, Zhang Y, Zhang T (2011) A highly active and sintering-resistant Au/FeO_x-hydroxyapatite catalyst for CO oxidation. Chem Commun (Camb) 47(6):1779–1781. https://doi.org/10.1039/c0cc04171h
13. Yan W, Brown S, Pan Z, Mahurin SM, Overbury SH, Dai S (2006) Ultrastable gold nanocatalyst supported by nanosized non-oxide substrate. Angew Chem Int Ed Engl 45(22):3614–3618. https://doi.org/10.1002/anie.200503808
14. Wang Y, B-b C, Crocker M, Y-j Z, X-b Z, Shi C (2015) Understanding on the origins of hydroxyapatite stabilized gold nanoparticles as high-efficiency catalysts for formaldehyde and benzene oxidation. Catal Commun 59:195–200. https://doi.org/10.1016/j.catcom.2014.10.028
15. Dick K, Dhanasekaran T, Zhang Z, Meisel D (2002) Size-dependent melting of silica-encapsulated gold nanoparticles. J Am Chem Soc 124(10):2312–2317. https://doi.org/10.1021/ja017281a
16. Zhang Y, Zhou Y, Zhang Z, Xiang S, Sheng X, Zhou S, Wang F (2014) Synthesis and characterization of a novel Au nanocatalyst with increased thermal stability. Dalton Trans 43(3):1360–1367. https://doi.org/10.1039/c3dt52108g
17. Xiang S, Zhou Y, Zhang Y, Zhang Z, Sheng X, Zhou S, Yang Z (2014) A highly reactive and enhanced thermal stability nanocomposite catalyst based on Au nanoparticles assembled in the inner surface of SiO_2 hollow nanotubes. Dalton Trans 43(28):11039–11047. https://doi.org/10.1039/c4dt00882k
18. Rashkeev SN, Dai S, Overbury SH (2010) Modification of Au/TiO_2 nanosystems by SiO_2 monolayers: toward the control of the Ccatalyst activity and stability. J Phys Chem C 114(7):2996–3002. https://doi.org/10.1021/jp9091738
19. del Río E, Hungría AB, Tinoco M, Manzorro R, Cauqui MA, Calvino JJ, Pérez-Omil JA (2016) CeO_2-modified Au/TiO_2 catalysts with outstanding stability under harsh CO oxidation conditions. Appl Catal B Environ 197:86–94. https://doi.org/10.1016/j.apcatb.2016.04.037
20. Puértolas B, Mayoral Á, Arenal R, Solsona B, Moragues A, Murcia-Mascaros S, Amorós P, Hungría AB, Taylor SH, García T (2015) High-temperature stable gold nanoparticle catalysts for application under severe conditions: the role of TiO_2 nanodomains in structure and activity. ACS Catal 5(2):1078–1086. https://doi.org/10.1021/cs501741u
21. Tang H, Liu F, Wei J, Qiao B, Zhao K, Su Y, Jin C, Li L, Liu JJ, Wang J, Zhang T (2016) Ultrastable hydroxyapatite/titanium-dioxide-supported gold nanocatalyst with strong metal-support interaction for carbon monoxide oxidation. Angew Chem Int Ed Engl 55(36):10606–10611. https://doi.org/10.1002/anie.201601823
22. Barrett DH, Scurrell MS, Rodella CB, Diaz B, Billing DG, Franklyn PJ (2016) Achieving nano-gold stability through rational design. Chem Sci 7(11):6815–6823. https://doi.org/10.1039/c6sc01597b
23. Tian C, Zhu X, Abney CW, Liu X, Foo GS, Wu Z, Li M, Meyer HM, Brown S, Mahurin SM, Wu S, Yang S-Z, Liu J, Dai S (2017) Toward the design of a hierarchical perovskite support: ultra-sintering-resistant gold nanocatalysts for CO oxidation. ACS Catal 7(5):3388–3393. https://doi.org/10.1021/acscatal.7b00483
24. Hemmingson SL, Campbell CT (2017) Trends in adhesion energies of metal nanoparticles on oxide surfaces: understanding support effects in catalysis and nanotechnology. ACS Nano 11:1196–1203. https://doi.org/10.1021/acsnano.6b07502

25. Ouyang R, Liu JX, Li WX (2013) Atomistic theory of Ostwald ripening and disintegration of supported metal particles under reaction conditions. J Am Chem Soc 135(5):1760–1771. https://doi.org/10.1021/ja3087054
26. Simakova IL, Solkina YS, Moroz BL, Simakova OA, Reshetnikov SI, Prosvirin IP, Bukhtiyarov VI, Parmon VN, Murzin DY (2010) Selective vapour-phase α-pinene isomerization to camphene over gold-on-alumina catalyst. Appl Catal, A 385(1–2):136–143. https://doi.org/10.1016/j.apcata.2010.07.002
27. Ivanova S, Petit C, Pitchon V (2006) Application of heterogeneous gold catalysis with increased durability: oxidation of CO and hydrocarbons at low temperature. Gold Bull 39(1):3–8. https://doi.org/10.1007/bf03215526
28. Gong J (2012) Structure and surface chemistry of gold-based model catalysts. Chem Rev 112(5):2987–3054. https://doi.org/10.1021/cr200041p
29. Abd El-Moemen A, Abdel-Mageed AM, Bansmann J, Parlinska-Wojtan M, Behm RJ, Kučerová G (2016) Deactivation of Au/CeO_2 catalysts during CO oxidation: influence of pretreatment and reaction conditions. J Catal 341:160–179. https://doi.org/10.1016/j.jcat.2016.07.005
30. Zanella R (2004) Characterization and reactivity in CO oxidation of gold nanoparticles supported on TiO_2 prepared by deposition-precipitation with NaOH and urea. J Catal 222(2):357–367. https://doi.org/10.1016/j.jcat.2003.11.005
31. Zanella R, Louis C (2005) Influence of the conditions of thermal treatments and of storage on the size of the gold particles in Au/TiO_2 samples. Catal Today 107-108:768–777. https://doi.org/10.1016/j.cattod.2005.07.008
32. Akita T, Lu P, Ichikawa S, Tanaka K, Haruta M (2001) Analytical TEM study on the dispersion of Au nanoparticles in Au/TiO_2 catalyst prepared under various temperatures. Surf Interface Anal 31(2):73–78. https://doi.org/10.1002/sia.959
33. Bore MT, Pham HN, Ward TL, Datye AK (2004) Role of pore curvature on the thermal stability of gold nanoparticles in mesoporous silica. Chem Commun (Camb) (22):2620–2621. https://doi.org/10.1039/b407575g
34. Yan X, Wang X, Tang Y, Ma G, Zou S, Li R, Peng X, Dai S, Fan J (2013) Unusual loading-dependent sintering-resistant properties of gold nanoparticles supported within extra-large mesopores. Chem Mater 25(9):1556–1563. https://doi.org/10.1021/cm303816g
35. Gabaldon JP, Bore M, Datye AK (2007) Mesoporous silica supports for improved thermal stability in supported Au catalysts. Top Catal 44(1–2):253–262. https://doi.org/10.1007/s11244-007-0298-4
36. Yan X, Wang X, Tang Y, Ma G, Zou S, Li R, Peng X, Dai S, Fan J (2013) Ordered, extra-large mesopores with highly loaded gold nanoparticles: a new sintering- and coking-resistant catalyst system. Chem Commun (Camb) 49(66):7274–7276. https://doi.org/10.1039/c3cc39196e
37. Bore MT, Pham HN, Switzer EE, Ward TL, Fukuoka A, Datye AK (2005) The role of pore size and structure on the thermal stability of gold nanoparticles within mesoporous silica. J Phys Chem B 109(7):2873–2880. https://doi.org/10.1021/jp045917p
38. Liu Z, Che R, Elzatahry AA, Zhao D (2014) Direct imaging Au nanoparticle migration inside mesoporous silica channels. ACS Nano 8(10):10455–10460. https://doi.org/10.1021/nn503794v
39. Zhu H, Liang C, Yan W, Overbury SH, Dai S (2006) Preparation of highly active silica-supported Au catalysts for CO oxidation by a solution-based technique. J Phys Chem B 110(22):10842–10848. https://doi.org/10.1021/jp060637q
40. Veith GM, Lupini AR, Rashkeev S, Pennycook SJ, Mullins DR, Schwartz V, Bridges CA, Dudney NJ (2009) Thermal stability and catalytic activity of gold nanoparticles supported on silica. J Catal 262:92–101
41. Hansen TW, Delariva AT, Challa SR, Datye AK (2013) Sintering of catalytic nanoparticles: particle migration or Ostwald ripening? Acc Chem Res 46(8):1720–1730. https://doi.org/10.1021/ar3002427
42. Wynblatt P, Gjostein NA (1975) Supported metal crystallites. Prog Solid State Chem 9:21–58. https://doi.org/10.1016/0079-6786(75)90013-8
43. Datye AK, Xu Q, Kharas KC, McCarty JM (2006) Particle size distributions in heterogeneous catalysts: what do they tell us about the sintering mechanism? Catal Today 111(1–2):59–67. https://doi.org/10.1016/j.cattod.2005.10.013
44. Munnik P, Velthoen ME, de Jongh PE, de Jong KP, Gommes CJ (2014) Nanoparticle growth in supported nickel catalysts during methanation reaction–larger is better. Angew Chem Int Ed Engl 53(36):9493–9497. https://doi.org/10.1002/anie.201404103
45. Rasmussen DB, Janssens TVW, Temel B, Bligaard T, Hinnemann B, Helveg S, Sehested J (2012) The energies of formation and mobilities of Cu surface species on Cu and ZnO in methanol and water gas shift atmospheres studied by DFT. J Catal 293:205–214. https://doi.org/10.1016/j.jcat.2012.07.001
46. Hugon A, Kolli NE, Louis C (2010) Advances in the preparation of supported gold catalysts: mechanism of deposition, simplification of the procedures and relevance of the elimination of chlorine. J Catal 274(2):239–250. https://doi.org/10.1016/j.jcat.2010.07.008
47. Prieto G, Zecevic J, Friedrich H, de Jong KP, de Jongh PE (2013) Towards stable catalysts by controlling collective properties of supported metal nanoparticles. Nat Mater 12(1):34–39. https://doi.org/10.1038/nmat3471
48. Delannoy L, El Hassan N, Musi A, Le To NN, Krafft JM, Louis C (2006) Preparation of supported gold nanoparticles by a modified incipient wetness impregnation method. J Phys Chem B 110(45):22471–22478. https://doi.org/10.1021/jp062130l
49. Dachille F, Sruousr PY, Roy R (1968) Pressure-temperature studies of anatase, brookite, rutile and TiO_2-II. Am Mineral 53:1929–1939
50. Tada K, Koga H, Hayashi A, Kondo Y, Kawakami T, Yamanaka S, Okumura M (2017) Theoretical clarification of the coexistence of Cl effects on Au/TiO2: the interaction between Au clusters and the TiO2 surface, and the aggregation of Au clusters on the TiO2 surface. Bull Chem Soc Jpn 90(5):506–519. https://doi.org/10.1246/bcsj.20160359
51. Farmer JA, Campbell CT (2010) Ceria maintains smaller metal catalyst particles by strong metal-support bonding. Science 329(5994):933–936. https://doi.org/10.1126/science.1191778
52. Harris PJF (2013) Growth and structure of supported metal catalyst particles. Int Mater Rev 40(3):97–115. https://doi.org/10.1179/imr.1995.40.3.97
53. Sehested J (2003) Sintering of nickel steam-reforming catalysts. J Catal 217(2):417–426. https://doi.org/10.1016/s0021-9517(03)00075-7
54. Campbell CT, Parker SC, Starr DE (2002) The effect of size-dependent nanoparticle energetics on catalyst sintering. Science 298(5594):811–814. https://doi.org/10.1126/science.1075094
55. Parker SC, Campbell CT (2007) Kinetic model for sintering of supported metal particles with improved size-dependent energetics and applications to Au onTiO_2(110). Phys Rev B 75(3). https://doi.org/10.1103/PhysRevB.75.035430
56. Prieto G, Meeldijk JD, de Jong KP, de Jongh PE (2013) Interplay between pore size and nanoparticle spatial distribution: consequences for the stability of CuZn/SiO_2 methanol synthesis catalysts. J Catal 303:31–40. https://doi.org/10.1016/j.jcat.2013.02.023
57. Parkinson GS, Novotny Z, Argentero G, Schmid M, Pavelec J, Kosak R, Blaha P, Diebold U (2013) Carbon monoxide-induced adatom sintering in a Pd-Fe_3O_4 model catalyst. Nat Mater 12(8):724–728. https://doi.org/10.1038/nmat3667
58. Ono LK, Roldan Cuenya B (2008) Formation and thermal stability of Au_2O_3 on gold nanoparticles: size and support effects. J Phys Chem C 112(12):4676–4686. https://doi.org/10.1021/jp711277u

59. Fujitani T, Nakamura I (2011) Mechanism and active sites of the oxidation of CO over Au/TiO_2. Angew Chem Int Ed Engl 50(43): 10144–10147. https://doi.org/10.1002/anie.201104694
60. Weiher N, Beesley AM, Tsapatsaris N, Delannoy L, Louis C, van Bokhoven JA, Schroeder SL (2007) Activation of oxygen by metallic gold in Au/TiO_2 catalysts. J Am Chem Soc 129(8):2240–2241. https://doi.org/10.1021/ja067316c
61. Kotobuki M, Leppelt R, Hansgen DA, Widmann D, Behm RJ (2009) Reactive oxygen on a Au/TiO_2 supported catalyst. J Catal 264(1):67–76. https://doi.org/10.1016/j.jcat.2009.03.013
62. Duan Z, Henkelman G (2015) CO oxidation at the Au/TiO_2 boundary: the role of the Au/Ti5c site. ACS Catal 5(3):1589–1595. https://doi.org/10.1021/cs501610a
63. Saavedra J, Doan HA, Pursell CJ, Grabow LC, Chandler BD (2014) The critical role of water at the gold-titania interface in catalytic CO oxidation. Science 345(6204):1599–1602. https://doi.org/10.1126/science.1256018
64. Comotti M, Li WC, Spliethoff B, Schuth F (2006) Support effect in high activity gold catalysts for CO oxidation. J Am Chem Soc 128(3):917–924. https://doi.org/10.1021/ja0561441
65. Date M, Okumura M, Tsubota S, Haruta M (2004) Vital role of moisture in the catalytic activity of supported gold nanoparticles. Angew Chem Int Ed Engl 43(16):2129–2132. https://doi.org/10.1002/anie.200453796
66. Haruta M (2003) When gold is not noble: catalysis by nanoparticles. Chem Rec 3(2):75–87. https://doi.org/10.1002/tcr.10053
67. Pougin A, Lüken A, Klinkhammer C, Hiltrop D, Kauer M, Tölle K, Havenith-Newen M, Morgenstern K, Grünert W, Muhler M, Strunk J (2017) Probing oxide reduction and phase transformations at the $Au\text{-}TiO_2$ interface by vibrational spectroscopy. Top Catal 60:1744–1753. https://doi.org/10.1007/s11244-017-0851-8
68. Lopez N, Norskov JK, Janssens TVW, Carlsson A, Puig-Molina A, Clausen BS, Grunwaldt JD (2004) The adhesion and shape of nanosized Au particles in a Au/TiO_2 catalyst. J Catal 225(1):86–94. https://doi.org/10.1016/j.jcat.2004.03.036
69. Schubert MM, Hackenberg S, van Veen AC, Muhler M, Plzak V, Behm RJ (2001) CO oxidation over supported gold catalysts—"inert" and "active" support materials and their role for the oxygen supply during reaction. J Catal 197(1):113–122. https://doi.org/10.1006/jcat.2000.3069
70. Masoud N, Delannoy L, Schaink H, van der Eerden A, de Rijk JW, Silva TAG, Banerjee D, Meeldijk JD, de Jong KP, Louis C, de Jongh PE (2017) Superior stability of Au/SiO_2 compared to Au/TiO_2 catalysts for the selective hydrogenation of butadiene. ACS Catal 7:5594–5603. https://doi.org/10.1021/acscatal.7b01424